# Sound radiation analysis with an enriched Timoshenko beam model based on second strain gradient theory

Guang Zhu, Abdelmalek Zine, Pascal Fossat, Mohamed Ichchou

# Sound radiation analysis with an enriched Timoshenko beam model based on second strain gradient theory

Guang Zhu[a], Abdelmalek Zine[b], Pascal Fossat[a], Mohamed Ichchou[a]

[a] *Vibroacoustics & Complex Media Research Group VIAME, LTDS - CNRS UMR 5513, Centre Lyonnais d'Acoustique CeLyA, École Centrale de Lyon, Université de Lyon, France*
[b] *Institute Camille Jordan – CNRS UMR 5208, École Centrale de Lyon, France*

**Abstract**

In this work, an enriched Timoshenko beam model describing non-classical bending and shear motion is employed to study its free wave propagation, frequency response, and sound radiation while considering the local behavior of its internal heterogeneity. The enriched Timoshenko beam model is established based on Mindlin's Second Strain Gradient (SSG) theory, which can capture the long-range interactions between underlying micro-structures in the frame of continuum mechanics. Dispersive behaviors of non-classical bending waves, shear waves, and the extra evanescent waves appearing exclusively in the SSG theory model are analyzed. Then investigations are carried forward into the modal density of non-classical bending waves, shear waves, and energy flow through the enriched model. At last, the frequency response and sound radiation of the Timoshenko beam are studied using wave approach based on its multi-modes character. The resulting non-classical frequency response and radiation features are compared with the classical elasticity theory result, upon which, impacts of local behavior in complex media on the structural dynamics and radiation features are discussed. The role of local behavior is, among others, clearly shown in the frame of the non-classical structural behavior.

*Keywords:* Second strain gradient theory, enriched Timoshenko beam model, wave propagation features, energy flow, frequency response, modal densities, sound radiation from non-local structure.

## 1. Introduction

Most materials used in the industry field, acquired from nature or manufactured artificially are heterogeneous materials. They have a rich and complicated internal structure, characterized by micro-structural details whose size typically ranges over many orders of magnitude. In classical formulations, material is assumed as a continuous media, and the stress in one point is assumed to depend on the strain at that point. However, for highly heterogeneous cases, constitutive models conceived for the conventional continuum become increasingly insufficient. This is particularly true for nano-scale structure deformation [1],

*mohamed.ichchou@ec-lyon.fr
*Email address:* mohamed.ichchou@ec-lyon.fr (Mohamed Ichchou)

and also true for a macroscopic structure that posses a different scale internal structure. The conventional continuum is only valid under long-wave approximation [2]. When the external wavelength is comparable with the characteristic size of heterogeneous features, *local behavior of the heterogeneity originating with the complex microstructure interactions plays a major role in characterizing the global behavior of the material.* In that case, local behavior and global behavior can be observed conjointly in the media, and that kind of media is defined as enriched complex media in what follows. It should be mentioned that the expression "micro-structure" in this work is used as a generic denomination for any type of internal material structure, not necessarily on the level of micrometers.

To describe the co-dynamic behavior (local and global) of multi-scale characters in complex media, one solution could be by developing the model with the combination of discrete material governed by the individual particles. The Molecular dynamics (MD) simulations approach is a candidate formulation. But MD simulation requires enormous time and computational resources, and still, its applications are limited to systems containing a relatively small number of molecules or atoms. As an alternative approach, generalized continuum theories based modeling have been developed in recent years, in which the local behavior of heterogeneity caused by long-range interactions can be described by inserting length scale parameters. Generalized theory can be categorized into three different branches: the higher gradient theory, the higher order theory, and non-local elasticity theories. Higher gradient theories (e.g. couple stress theory [3], strain gradient theory [4], second strain gradient theory [5]) generalized the classical continuum theory by enriching potential energy with higher order gradients of strain. Higher order theories (e.g. micropolar theory, micromorphic theory [6] are developed by supplying additional degrees of freedom to a material point which can describe the effects of the underlying micro-structure deformation. The nonlocal elasticity theories [7] generalized the classical theory by associating the stress in one point directly to the strain of a certain neighborhood of that point or even of the entire body.

Generalized continuum elasticity theory has been employed by many researchers in complex media modeling in short wave limits. One of its pioneering applications lays in the investigation of size-dependence character and non-local behavior in nano-size structures, see [8, 9, 10, 4]. In addition to the distinct influences on structural static and free vibration characteristics, local behavior in complex media caused by non-local interaction between internal structures also leads to high complexity in wave propagation. Some pioneering investigations have also been proceeded in this field by employing the generalized continuum theory modeling. Recent work by Suiker et al. [11, 12] predicted 'dispersive' body waves based on the proposed second-gradient micro-polar formulation, and its dispersion becomes more prominent when the wavelength reaches the order the particle size. Wave propagation characteristics are also investigated by Gopalakrishnan [13] with using the Erigen's Stress Gradient model and Mindlin's Strain Gradient model, by Li et al. [14] with using non-local strain gradient theory model. Length scale parameters are brought into the continuum governing equations, and these scale parameters are proven to be significantly affecting

the wave propagation features. In the work of Metrikin and Askes [15, 16], they suggested a dynamically consistent gradient model in which each higher-order stiffness term is accompanied by a higher order inertia term. The resulting dispersion equation suggested that one harmonic vibration of a point of this model perturbs three 'waves' (one propagating and two oscillations) from each side of this point.

However, it should be mentioned that this rich and abundant literature belonging to the development of sophisticated models is rarely considered in the vibration and acoustic community. Indeed, most structural models of use in the Noise and Vibration Harshness studies belong to classical or conventional theory class. The reason is simple. The enriched model is sometimes hard to justify for the modeling of employed materials in some sectors. Some of these enriched models did not yet completely convince engineers and designers about their intrinsic interest. This trend is expected however to reverse in the few coming periods. Most mechanical construction developers are looking for lightweight materials for obvious ecological and economical reasons. Most of these lightweight materials are composite made with more and more sophisticated architecture. The emergence of the metamaterial and metastructure way of thinking is rapidly reinforcing this way of thinking. The present part is then a modest contribution to the use of the enriched models in vibration and acoustics. The issue of wave propagation, as well as noise radiated from such complex structures, is specifically studied. The main focus is the comparison between classical theories and non-classical ones. *The main question being, how local behavior affects the vibroacoustic indicators and for which expected benefit?.*

Since the long-range interaction in one-dimensional structure is easier to understand and interpret, the investigation starts from the beam structure. In analyses of beam-like structures, two theories are usually employed, namely Euler–Bernoulli theory and Timoshenko beam theories, and upon the classical theories modified higher order beam theories have also been developed [17, 18]. Indeed, as shear effect is evident for enriched media [7], higher order beam theories are more favorable. Consider the complexity and accuracy of the model, classical Timoshenko beam theory is applied in this work. The Second strain gradient (SSG) theory based Timoshenko beam model, developed by Asghari [19], is employed to investigate the wave propagation features considering the local behavior of internal heterogeneity caused by long-range interactions. The governing equation and associated boundary conditions are normalized in Sec. 2, then the dispersive behavior of wave modes in the non-local media is analyzed in Sec. 3.1. Subsequently, modal densities of the propagating wave modes (Sec.3.2) and energy flow through the structure are calculated (Sec.3.3). Upon which, Frequency Response Functions (FRF) of the non-classical Timoshenko beam is investigated in Sec.4. Sound radiation from the vibrating surface of the structure is derived in 4 in terms of its normal square velocity, radiation impedance, and radiated pressure field. Numerical applications and result discussions are presented in Sec. 6 and conclusions are drawn in Sec. 7. This work is not only a contribution to the analysis of wave propagation and radiation of complex media but also aims at providing an original solution to analyze the wave propagation and radiation characteristics of complex media with micro-scale periodicity.

## 2. Normalized governing equations and boundary conditions

The research object considered in what follows is an SSG theory-based Timoshenko one. Taking into account the bending motion allows a generic vibroacoustic analysis to be conducted while keeping the analytical and numerical reasoning. Deriving analytical expressions for the dynamic indicators when possible allows comprehensive comparisons between classical and non-classical theories. Considering the Timoshenko beam with a rectangular section, the coordinate system $x-y-z$ and kinematic parameters of the model are illustrated in Figure 1 with its $x$-axis along the axial direction of the beam, and its origin on the left-end section. The plane $x-y$ of the coordinate system is coincident with the mid-plane of the beam. The beam is assumed to be uniform, homogeneous, and initially straight along the $x$-direction with length $L$, and the cross-section is assumed to remain plane after deformation. $q\left(x,t\right)$ denotes the distributed loads acting on the beam in the transverse direction as force per unit axial length.

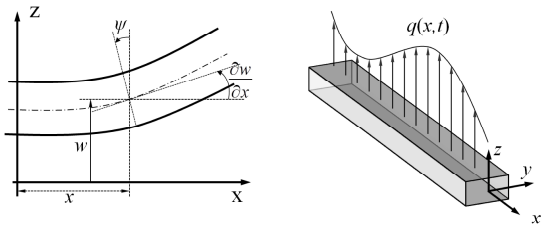


Figure 1: The coordinate system and kinematic parameters of the enriched Timoshenko beam model

The components of the displacement field in the enriched Timoshenko beam model in an in-plane motion are written as

$$\begin{aligned} u_x\left(x,y,z,t\right) &= -z\,\psi\left(x,t\right), \\ u_y\left(x,y,z,t\right) &= 0, \\ u_z\left(x,y,z,t\right) &= w\left(x,t\right), \end{aligned} \tag{1}$$

where $u_x$, $u_y$, and $u_z$ denote the displacement of the beam particles along $x$, $y$, and $z$ directions respectively. $w(x,t)$ represents the flexural deformation of the beam. The cross-sections are not assumed to remain perpendicular to the deformed axial line of the beam, instead $\psi(x,t)$ represents the rotation angle of the cross-sections after deformation with respect to the perpendicular section.

With Mindlin's SSG theory, the potential energy density is generalized with higher order strain components as in Eq. (2).

$$\begin{aligned} \bar{u} =& \frac{1}{2}\lambda\varepsilon_{ii}\varepsilon_{jj} + \mu\varepsilon_{ij}\varepsilon_{ij} + a_1\eta_{ijj}\eta_{ikk} + a_2\eta_{iik}\eta_{kjj} + a_3\eta_{iik}\eta_{jjk} + a_4\eta_{ijk}\eta_{ijk} + a_5\eta_{ijk}\eta_{kji} \\ &+ b_1\xi_{iijj}\xi_{kkll} + b_2\xi_{ijkk}\xi_{ijll} + b_3\xi_{iijk}\xi_{jkll} + b_4\xi_{iijk}\xi_{llkj} + b_5\xi_{iijk}\xi_{lljk} + b_6\xi_{ijkl}\xi_{ijkl} \\ &+ b_7\xi_{ijkl}\xi_{jkli} + c_1\varepsilon_{ii}\xi_{jjkk} + c_2\varepsilon_{ij}\xi_{ijkk} + c_3\varepsilon_{ij}\xi_{kkij} + b_0\varepsilon_{iijj}, \end{aligned} \tag{2}$$

where $\lambda$ and $\mu$ are the Lame's constants. Parameters $a_i$, $b_i$ and $c_i$ are sixteen higher-order material constants which particularly appear in SSG theory. $\varepsilon_{ij}$, $\eta_{ijk}$ and $\xi_{ijkl}\,(i,j,k,l=1,2,3)$ are the components of strain tensors $\boldsymbol{\varepsilon}$, $\boldsymbol{\eta}$ and $\boldsymbol{\xi}$, their expressions can be written in terms of the gradient of displacement vector $\mathbf{u}$ as

$$\varepsilon_{ij}=\frac{1}{2}\left[\nabla\mathbf{u}+\mathbf{u}\nabla\right]_{ij}, \quad \eta_{ijk}=\left[\nabla\nabla\mathbf{u}\right]_{ijk}, \quad \xi_{ijkl}=\left[\nabla\nabla\nabla\mathbf{u}\right]_{ijkl}. \tag{3}$$

Substitution of the motion equations into the potential energy density gives the enriched potential energy, and the governing equations can be obtained by applying Hamilton principle [19]. For parametric study of the wave propagation behavior in higher frequency, the following dimensionless variables are defined as,

$$\overline{x}=\frac{x}{L}, \quad \overline{w}=\frac{w}{L}, \quad \overline{\omega}=\frac{\omega}{\omega_k}, \quad \tau=\frac{t}{t_k} \tag{4}$$

in which, the frequency normalization term $\omega_k=\sqrt{\frac{Ak'\mu}{I\rho}}$ is the cut-on frequency of the shear wave in classical Timoshenko beam theory, and $k'$ is the shear constant depending on the shape of cross sections. The normalization parameter for time $t$ $t_k=\frac{1}{\omega_k}=\sqrt{\frac{I\rho}{Ak'\mu}}$. With the newly defined variables, normalized governing equations of motion can be written as,

$$\begin{aligned}
&-\psi+\left(\frac{B_1-2c_2A-Ac_3}{\mu AL^2}\right)\left(\frac{\partial^2\psi}{\partial\overline{x}^2}\right)+\left(\frac{B_4-B_2}{\mu AL^4}\right)\left(\frac{\partial^4\psi}{\partial\overline{x}^4}\right)+\frac{B_3}{\mu AL^6}\frac{\partial^6\psi}{\partial\overline{x}^6}+\frac{\partial\overline{w}}{\partial\overline{x}}\\
&\quad+\left(\frac{B_7+2\left(c_2+c_3\right)A}{2\mu AL^2}\right)\left(\frac{\partial^3\overline{w}}{\partial\overline{x}^3}\right)-\frac{B_8}{2\mu AL^4}\frac{\partial^5\overline{w}}{\partial\overline{x}^5}=\frac{m_2}{\mu A{t_k}^2}\frac{\partial^2\psi}{\partial\tau^2}\\
&-\left(\frac{\partial\psi}{\partial\overline{x}}\right)-\left(\frac{B_7+2\left(c_3+c_2\right)A}{2\mu AL^2}\right)\left(\frac{\partial^3\psi}{\partial\overline{x}^3}\right)+\frac{B_8}{2\mu AL^4}\left(\frac{\partial^5\psi}{\partial\overline{x}^5}\right)+\left(\frac{\partial^2\overline{w}}{\partial\overline{x}^2}\right)\\
&\quad+\left(\frac{c_3A-B_5}{\mu AL^2}\right)\left(\frac{\partial^4\overline{w}}{\partial\overline{x}^4}\right)+\frac{B_6}{\mu AL^4}\left(\frac{\partial^6\overline{w}}{\partial\overline{x}^6}\right)+\overline{q}=\frac{m_0L^2}{\mu A{t_k}^2}\left(\frac{\partial^2\overline{w}}{\partial t^2}\right)
\end{aligned} \tag{5}$$

in which $\overline{q}=qL/\mu A$ is the dimensionless body load intensity, $m_0=\rho A$, $m_2=\rho\int_A z^2dA$, and $B_i$ represents the higher order material constant factors as

$$\begin{aligned}
&B_1=\zeta EI+2A(a_1+2a_4+a_5),\\
&B_2=2I(a_1+a_2+a_3+a_4+a_5)+2A(2b_2+b_3+b_5+3b_6+2b_7),\\
&B_3=2I(b_1+b_2+b_3+b_4+b_5+b_6+b_7)\\
&B_4=2I(c_1+c_2+c_3),B_5=2A(a_3+a_4), \qquad B_6=2A(b_5+b_6),\\
&B_7=-2A(a_2+2a_5), \qquad B_8=-2A(b_3+2b_4+2b_7),
\end{aligned}$$

with parameter $A$ as the area of the beam cross section, and $I=\int_A z^2dA$ as the area moment of inertia for the beam cross section around $y$ axis. To avoid the influence of Poisson effect, $\zeta=1$ is set.

With the same normalization parameters, the dimensionless boundary conditions are obtained as,

$$
\begin{aligned}
\overline{M}_0 =& \left(\frac{2B_1-2c_2A-c_3A}{2\mu AL^2}\right)\left(\frac{\partial\psi}{\partial\overline{x}}\right)+\left(\frac{B_4-B_2}{\mu AL^4}\right)\left(\frac{\partial^3\psi}{\partial\overline{x}^3}\right)+\frac{B_3}{\mu AL^6}\left(\frac{\partial^5\psi}{\partial\overline{x}^5}\right)\\
&+\left(\frac{B_7+2c_2A+c_3A}{2\mu AL^2}\right)\left(\frac{\partial^2\overline{w}}{\partial\overline{x}^2}\right)-\frac{B_8}{2\mu AL^4}\left(\frac{\partial^4\overline{w}}{\partial\overline{x}^4}\right) \qquad or\ \ \delta\psi=0\\
\overline{M}_1 =& \left(\frac{2c_2+c_3}{2\mu L^2}\right)\psi+\left(\frac{2B_2-B_4}{2\mu AL^4}\right)\left(\frac{\partial^2\psi}{\partial\overline{x}^2}\right)-\frac{B_3}{\mu AL^6}\left(\frac{\partial^4\psi}{\partial\overline{x}^4}\right)-\left(\frac{2c_2+c_3}{2\mu L^2}\right)\left(\frac{\partial\overline{w}}{\partial\overline{x}}\right)\\
&+\frac{B_8}{2\mu AL^4}\left(\frac{\partial^3\overline{w}}{\partial\overline{x}^3}\right) \qquad or\ \ \delta\left(\frac{\partial\psi}{\partial\overline{x}}\right)=0\\
\overline{M}_2 =& \frac{B_4}{2\mu AL^4}\left(\frac{\partial\psi}{\partial\overline{x}}\right)+\frac{B_3}{\mu AL^6}\left(\frac{\partial^3\psi}{\partial\overline{x}^3}\right) \qquad or\quad \delta\left(\frac{\partial^2\psi}{\partial\overline{x}^2}\right)=0\\
\overline{V}_0 =& -\psi-\left(\frac{B_7+2\left(c_3+c_2\right)A}{2\mu AL^2}\right)\left(\frac{\partial^2\overline{w}}{\partial\overline{x}^2}\right)+\frac{B_8}{2\mu AL^4}\left(\frac{\partial^4\psi}{\partial\overline{x}^4}\right)+\left(\frac{\partial\overline{w}}{\partial\overline{x}}\right)\\
&+\left(\frac{c_3A-B_5}{\mu AL^2}\right)\left(\frac{\partial^3\overline{w}}{\partial\overline{x}^3}\right)+\frac{B_6}{\mu AL^4}\left(\frac{\partial^5\overline{w}}{\partial\overline{x}^5}\right) \quad or\ \ \delta\overline{w}=0\\
\overline{V}_1 =& \left(\frac{B_7+c_3A}{2\mu AL^2}\right)\left(\frac{\partial\psi}{\partial\overline{x}}\right)-\frac{B_8}{2\mu AL^4}\left(\frac{\partial^3\psi}{\partial\overline{x}^3}\right)+\left(\frac{B_5-c_3A}{\mu AL^2}\right)\left(\frac{\partial^2\overline{w}}{\partial\overline{x}^2}\right)-\frac{B_6}{\mu AL^4}\left(\frac{\partial^4\overline{w}}{\partial\overline{x}^4}\right)\\
&\qquad\qquad\qquad\qquad\qquad\qquad or\quad \delta\left(\frac{\partial\overline{w}}{\partial\overline{x}}\right)=0\\
\overline{V}_2 =& -\frac{c_3}{2\mu L^2}\psi+\frac{B_8}{2\mu AL^4}\left(\frac{\partial^2\psi}{\partial\overline{x}^2}\right)+\frac{c_3}{2\mu L^2}\left(\frac{\partial\overline{w}}{\partial\overline{x}}\right)+\frac{B_6}{\mu AL^4}\left(\frac{\partial^3\overline{w}}{\partial\overline{x}^3}\right) \quad or\quad \delta\left(\frac{\partial^2\overline{w}}{\partial\overline{x}^2}\right)=0
\end{aligned}
\tag{6}
$$

## 3. Analysis of wave dispersion characteristics, modal density and energy flow

### 3.1. Dispersion relation

For media with internal heterogeneity due to micro-structures effects, classical elasticity theory is not capable of describing their deformation behavior and capturing their wave dispersion properties especially when the wavelength is of the same order with the major heterogeneity. This phenomenon has been illustrated in the research of Zhu et al. [20] for non-local rod structures. In this section, dispersion relation of free waves propagating in enriched Timoshenko beam model is investigated based on the proposed model.

Assuming the external loading $\overline{q}=0$, free wave propagation modes in enriched model can be achieved by substituting the general exponential form of wave propagation solution:

$$
\begin{aligned}
w(x,t) &= w_0 e^{i(\omega t-kx)}\\
\psi(x,t) &= \psi_0 e^{i(\omega t-kx)}
\end{aligned}
\tag{7}
$$

into the governing equations ($k$ indicating wavenumber and $\omega$ angular frequency), then we have

$$
\begin{aligned}
\mathcal{R}\psi_0+\mathcal{S}w_0=0,\\
\mathcal{S}\psi_0+\mathcal{T}w_0=0,
\end{aligned}
\tag{8}
$$

in which,

$$\mathcal{R} = -B_3k^6 + (-B_2 + B_4)\,k^4 + (2\,Ac_2 + Ac_3 - B_1)\,k^2 + m_2\omega^2 - \mu A,$$
$$\mathcal{S} = \frac{B_8}{2}ik^5 + \left(\frac{B_7}{2} + Ac_2 + Ac_3\right)ik^3 - i\mu Ak,$$
$$\mathcal{T} = B_6k^6 + (-Ac_3 + B_5)\,k^4 + \mu Ak^2 - m_0\omega^2.$$

In order to have nontrivial solutions for $\psi_0$ and $w_0$ in Eq. (8), the determinant of coefficients must be zero, consequently one 12th-order function with respect of wavenumber $k$ is obtained as the dispersion relation for the enriched Timoshenko beam model,

$$k_{12}k^{12} + k_{10}k^{10} + k_8k^8 + k_6k^6 + k_4k^4 + k_2k^2 + k_0 = 0 \tag{9}$$

in which,

$$k_{12} = -B_3B_6; \qquad k_{10} = \tfrac{{B_8}^2}{4} - B_3B_5 + (B_4 - B_2)\,B_6 + c_3AB_3;$$
$$k_8 = B_4B_5 - B_2B_5 - B_1B_6 + \tfrac{B_7B_8}{2} + c_3A\,(B_2 - B_4 + B_6 + B_8) + 2c_2AB_6 + c_2AB_8 - \mu AB_3;$$
$$k_6 = \tfrac{{B_7}^2}{4} + A^2{c_2}^2 - B_1B_5 + c_2A\,(2B_5 + B_7) + c_3A\,(B_1 + B_5 + B_7)$$
$$- A\mu\,(B_2 - B_4 + B_6 - B_8) + \omega^2\,(B_3m_0 + B_6m_2)\,;$$
$$k_4 = m_0\omega^2\,(B_2 - B_4) + m_2\omega^2\,(B_5 - c_3A) - A\mu\,(B_5 + B_7 + B_1)\,;$$
$$k_2 = m_0\omega^2\left(B_1 - 2c_2A - c_3A + \tfrac{m_2}{m_0}\mu A\right); \qquad k_0 = m_0\omega^2\left(A\mu - m_2\omega^2\right).$$

This dispersion equation is a 12th-order function concerning wavenumber, thus 12 wave modes can be generated in the enriched Timoshenko beam model, among which 6 are positive-going wave and 6 are negative-going waves. For parametric study, wavenumber is normalized with $\overline{k} = kL$, then the normalized dispersion relation is displayed as,

$$\overline{k}_{12}\overline{k}^{12} + \overline{k}_{10}\overline{k}^{10} + \overline{k}_8\overline{k}^8 + \overline{k}_6\overline{k}^6 + \overline{k}_4k^4 + \overline{k}_2\overline{k}^2 + \overline{k}_0 = 0 \tag{10}$$

in which,

$$\overline{k}_{12} = -\tfrac{k_{12}}{L^{10}}; \quad \overline{k}_{10} = \tfrac{k_{10}}{L^8}; \quad \overline{k}_8 = \tfrac{k_8}{L^6}; \quad \overline{k}_2 = \tfrac{k_2}{{t_k}^2}; \quad \overline{k}_0 = \tfrac{L^2}{{t_k}^2}k_0.$$
$$\overline{k}_6 = \tfrac{1}{L^4}\left[\tfrac{{B_7}^2}{4} + A^2{c_2}^2 - B_1B_5 + 2c_2AB_5 + c_2AB_7 + c_3A\,(B_1 + B_5 + B_7)\right]$$
$$- \tfrac{A\mu}{L^4}\,(B_2 - B_4 + B_6 - B_8) + \tfrac{\omega^2}{{t_k}^2L^4}\,(B_3m_0 + B_6m_2)\,;$$
$$\overline{k}_4 = \tfrac{m_0\omega^2}{{t_k}^2L^2}\,(B_2 - B_4) + \tfrac{m_2\omega^2}{{t_k}^2L^2}\,(B_5 - c_3A) - \tfrac{A\mu}{L^2}\,(B_5 + B_7 + B_1)\,;$$

### *3.2. Modal density*

Modal density $n\,(\omega)$ of a structure indicates the number of resonant frequencies in a neighborhood $\Delta\omega$ local to frequency $\omega$. It may also be interpreted as the expected number of natural frequencies per radiant per second as

$$n(\omega) = \frac{dN}{d\omega}, \tag{11}$$

in which $N$, the mode count, represents the number of resonant frequencies below that given frequency $\omega$. Assuming $\delta$ represent the total phase change introduced by reflecting boundaries which varies with different boundary conditions, then based on the 'phase-closure principle' the relation between wavenumber and mode count for the studied beam of length $L$ can be expressed as

$$2kL \pm \delta = N \cdot 2\pi \Rightarrow N(k) = \frac{kL \pm \delta}{\pi}.$$

As the mode order increases, the number of resonances $N(k)$ in frequency domain become increasingly less sensitive to the boundary conditions. Hence, we may consider the mode count as,

$$N(k) = \frac{kL}{\pi}, \tag{12}$$

and Eq. (11) can be simplified as

$$n(\omega) = \frac{dN}{d\omega} = \frac{dN}{dk}\frac{dk}{d\omega} = \frac{L}{\pi}\frac{1}{C_g}, \tag{13}$$

in which, the term $C_g$ denotes the group velocity of the studied wave mode, and it represents information and energy transported velocity by this wave mode.

### *3.3. Energy flow*

In enriched Timoshenko beam model, energy flow can be carried away by all the six wave modes. For further exploration in FRF and vibration radiation, energy velocity at one point in the studied enriched model is formulated in this section. At one observation point $M$, the instantaneous kinetic energy density $\mathrm{T(M,t)}$, is defined [21] as

$$\mathrm{T} = \frac{\rho}{2}\mathrm{Re}\left(\mathbf{V}\right) \cdot \mathrm{Re}\left(\mathbf{V}\right). \tag{14}$$

where $\mathbf{V}$ is velocity vector. As the strain and stress tensors are defined differently in SSG theory, potential energy density and energy flow should be revised accordingly. The potential energy density $\mathrm{U(M,t)}$ of the studied model is enriched with the higher order components as in equation (2). The sum of the kinetic and potential energy density yields the instantaneous total energy density as:

$$\mathrm{W_{total}} = \mathrm{T} + \mathrm{U}. \tag{15}$$

For a vibrating structure, the time averaged value is more important than the instantaneous value. In the following investigations, the time will be removed. A physical quantity $H$, which represents here an energy or a power density, can generally be expressed as

$$H = f \cdot g,$$

where $f$ and $g$ are complex harmonic physical variables denoting stress, strain, or displacement in the formulation. Thus the time averaging of $H$ is given by

$$\langle H\rangle = \frac{\omega}{2\pi}\int_0^{2\pi} \mathrm{Re}\,(f)\cdot \mathrm{Re}\,(g)dt = \frac{1}{2}\mathrm{Re}\,(f\cdot g^*)\,,$$

where '*' denotes complex conjugation, and '$\langle\ \rangle$' denotes time averaged. For the studied beam model, time averaged kinetic energy and time averaged potential energy per unit length can be deduced as

$$\begin{aligned}
\langle \mathrm{T}\rangle &= \frac{\rho}{4}\int_A \left[\mathrm{Re}\,(\dot{w}\cdot\dot{w}^*) + z^2\cdot \mathrm{Re}\left(\dot{\psi}\cdot\dot{\psi}^*\right)\right] dA,\\
\langle \mathrm{U}\rangle &= \frac{1}{4}\mathrm{Re}\left[B_1\left(\frac{\partial\psi}{\partial x}\right)\left(\frac{\partial\psi}{\partial x}\right)^* + B_2\left(\frac{\partial^2\psi}{\partial x^2}\right)\left(\frac{\partial^2\psi}{\partial x^2}\right)^* + B_3\left(\frac{\partial^3\psi}{\partial x^3}\right)\left(\frac{\partial^3\psi}{\partial x^3}\right)^*\right.\\
&\quad + B_4\left(\frac{\partial\psi}{\partial x}\right)\left(\frac{\partial^3\psi}{\partial x^3}\right)^* + B_5\left(\frac{\partial^2 w}{\partial x^2}\right)\left(\frac{\partial^2 w}{\partial x^2}\right)^* + B_6\left(\frac{\partial^3 w}{\partial x^3}\right)\left(\frac{\partial^3 w}{\partial x^3}\right)^*\\
&\quad + B_7\left(\frac{\partial\psi}{\partial x}\right)\left(\frac{\partial^2 w}{\partial x^2}\right)^* + B_8\left(\frac{\partial^2\psi}{\partial x^2}\right)\left(\frac{\partial^3 w}{\partial x^3}\right)^* + A\mu\left(\frac{\partial w}{\partial x}-\psi\right)\left(\frac{\partial w}{\partial x}-\psi\right)^*\\
&\quad \left. -2c_2A\left(\frac{\partial w}{\partial x}-\psi\right)\left(\frac{\partial^2\psi}{\partial x^2}\right)^* + c_3A\left(\frac{\partial w}{\partial x}-\psi\right)\left(\frac{\partial^3 w}{\partial x^3}-\frac{\partial^2\psi}{\partial x^2}\right)^*\right],
\end{aligned} \tag{16}$$

in which '$\dot{w}$' '$\dot{\psi}$' denote the time derivative of $w$ and $\psi$. The instantaneous active energy flow $\mathrm{P}_0$ for the classical elasticity theory are defined [22] as

$$\mathrm{P}_0 = -\mathrm{Re}\,(\boldsymbol{\sigma})\cdot \mathrm{Re}\,(\mathbf{V})\,,$$

which is the power done by the stress $\sigma$. For the enriched Timoshenko beam model, power can be applied not only through the classical stress $\sigma$ but also the higher order stresses $\boldsymbol{\tau}$ and $\boldsymbol{\eta}$. After integrating through the observation section, the expression of time averaging active energy flow per unit length is assumed in form of

$$\langle \mathrm{P}\rangle = -\frac{1}{2}\mathrm{Re}\left[V_0\cdot\dot{w}^* + V_1\cdot\left(\frac{\partial\dot{w}}{\partial x}\right)^* + V_2\cdot\left(\frac{\partial^2\dot{w}}{\partial x^2}\right)^* + M_0\cdot\dot{\psi}^* + M_1\cdot\left(\frac{\partial\dot{\psi}}{\partial x}\right)^* + M_2\cdot\left(\frac{\partial^2\dot{\psi}}{\partial x^2}\right)^*\right], \tag{17}$$

where $V_0$, $V_1$, $V_2$ and $M_0$, $M_1$, and $M_2$ are the loads dual to the corresponding kinematic parameters. They are resultants of not only classical stress but also higher-order stresses. $V_0$ and $M_0$ are referred as shear force and bending moment acting on the end sections. $V_1$ and $M_1$ denote the first higher-order loads with unit of $\mathrm{N}\cdot\mathrm{m}$ and $\mathrm{N}\cdot\mathrm{m}^2$, and $V_2$ and $M_2$ denote the second higher-order loads with unit of $\mathrm{N}\cdot\mathrm{m}^2$ and $\mathrm{N}\cdot m^3$. They are related with the displacement and derivatives of displacement at $M$ position as in Eq.(6).

Meanwhile energy velocity through the enriched Timoshenko beam model equals the time averaged active energy flow $\langle P\rangle$ over the time averaged total energy $\langle W_{total}\rangle$ as

$$\mathrm{V}_e = \frac{\langle \mathrm{P}\rangle}{\langle W_{total}\rangle}. \tag{18}$$

In the numerical study, the formulated expressions of energy flow and potential energy density will be verified by the following theorem. *When there is only one conservative wave propagating in the complex structure, energy velocity* $\mathrm{V}_e$ *obtained by the above formulation should be equal with the group velocity of that wave* $C_g$.

## 4. Frequency response function analysis

Frequency response analysis of the Timoshenko beam subject to a harmonic excitation and certain boundary condition is investigated in this section. The studied cantilever bean is fixed at left-end, and subject to a harmonic force $F = \mathrm{Re}\left\{q_0 e^{i\omega t}\right\}$ as shown Figure 2. The height of the cross-section is $h$, width $b$, and the length of the beam is $L$. The observation point can be at any position, in this case, it is set to be at $x = 0.7L$. The investigation is done with wave approach and the result are verified with Finite Element Method (in Appendix).

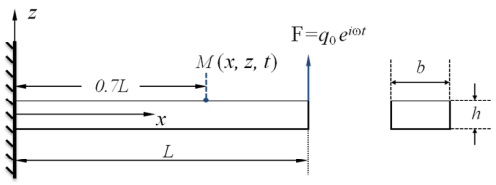


Figure 2: A fixed-free Timoshenko beam with loading in free end

Based on the previously obtained wave modes in section 3.1, the solution for the displacement field can be given by the superposition of all the progressive and retrograde waves ($\pm\overline{k}_1$, $\pm\overline{k}_2$, $\pm\overline{k}_3$, $\pm\overline{k}_4$, $\pm\overline{k}_5$, $\pm\overline{k}_6$). With wave approach, the general expressions of the dimensionless displacement $\overline{w}$ and $\overline{\psi}$ can be expressed as

$$\begin{aligned}\overline{w}(\bar{x},\tau) &= \left(\sum_{i=1}^{6}\mathcal{A}_i e^{-i\bar{k}_i\bar{x}} + \sum_{i=1}^{6}\mathcal{B}_i e^{i\bar{k}_i\bar{x}}\right)\cdot e^{i\overline{\omega}\tau},\\ \psi(\bar{x},\tau) &= \left(\sum_{i=1}^{6}\mathcal{C}_i e^{-i\bar{k}_i\bar{x}} + \sum_{i=1}^{6}\mathcal{D}_i e^{i\bar{k}_i\bar{x}}\right)\cdot e^{i\overline{\omega}\tau},\end{aligned} \tag{19}$$

To calculate the amplitudes in Eq. (19), boundary conditions at each end are required. There are two kinds of conditions: a loading type and a geometric type, and only one kind need to be satisfied for each kinetic parameter. For the case in Figure 2, the generalized loading type and geometric type boundary conditions are expressed in Eq. (20)

$$\begin{aligned}\overline{w}\,(0,\overline{\omega}) &= 0; & \overline{V}_0\,(1,\overline{\omega}) &= -\overline{q_0};\\ \psi\,(0,\overline{\omega}) &= 0; & \overline{M}_0\,(1,\overline{\omega}) &= 0;\\ \overline{V}_1\,(0,\overline{\omega}) &= 0; & \overline{V}_1\,(1,\overline{\omega}) &= 0;\\ \overline{M}_1\,(0,\overline{\omega}) &= 0; & \overline{M}_1\,(1,\overline{\omega}) &= 0;\\ \overline{V}_2\,(0,\overline{\omega}) &= 0; & \overline{V}_2\,(1,\overline{\omega}) &= 0;\\ \overline{M}_2\,(0,\overline{\omega}) &= 0; & \overline{M}_2\,(1,\overline{\omega}) &= 0;\end{aligned} \tag{20}$$

where $\overline{q}_0 = \frac{q_0}{\mu A}$ denotes the normalized amplitude of harmonic excitation force. Physically speaking, the extra kinematic parameters $\frac{\partial w}{\partial x}$, $\frac{\partial^2 w}{\partial x^2}$ and $\frac{\partial \psi}{\partial x}$, $\frac{\partial^2 \psi}{\partial x^2}$ represent the inner relative movement of the adjacent micro-structures. The higher-order generalized loads represent the inner interactions between the adjacent micro-structures generated by variation of the inner relative movement. At the fixed end $\overline{x} = 0$, transverse displacement $\overline{w}$ and rotation angle $\psi$ equal zero; The higher-order generalized forces $\overline{V}_1$, $\overline{V}_2$ and $\overline{M}_1$, $\overline{M}_2$ are set to be zero since the forces that possibly produced by the fixed base are only classical shear force and bending moment. At the force excitation end $\overline{x} = 1$, the produced classical force and moment $\overline{V}_0$ and $\overline{M}_0$ follow the equilibrium for shear force and bending moment. The higher-order forces $\overline{V}_1$, $\overline{V}_2$ and $\overline{M}_1$, $\overline{M}_2$ are set to be zero.

The above 12 equations are not sufficient to calculate the 24 variables in the solution (19). But we also know that the general solution form of $\overline{w}$ and $\psi$ should be valid to the governing Eqs. (5) on any frequency $\overline{\omega}$ for all the point $\overline{x}$ on the structure except the boundary points. Hence when substitute the solution of Eq. (19) into the governing equations, the coefficient of each term $e^{\pm i\overline{k}_i\overline{x}+i\overline{\omega}\tau}$ should equal zero, which yields amplitudes of $\overline{w}$ and $\psi$ for each mode following the principles as

$$\begin{aligned}
\mathcal{C}_i &= \frac{-2i\left(-B_6\bar{k}_t^2\bar{k}_i^6 + c_3AL^2\bar{k}_t^2\bar{k}_i^4 - B_5L^2\bar{k}_t^2\bar{k}_i^4 - \mu AL^4\bar{k}_t^2\bar{k}_i^2 + m_0\omega^2L^6\right)}{\bar{k}_i\bar{k}_t^2\left(B_8\bar{k}_i^4 + 2c_2AL^2\bar{k}_i^2 + 2c_3AL^2\bar{k}_i^2 + B_7L^2\bar{k}_i^2 - 2\mu AL^4\right)}\mathcal{A}_i; \quad (i = 1, 2, 3, ...6) \\
\mathcal{D}_i &= \frac{2i\left(-B_6\bar{k}_t^2\bar{k}_i^6 + c_3AL^2\bar{k}_t^2\bar{k}_i^4 - B_5L^2\bar{k}_t^2\bar{k}_i^4 - \mu AL^4\bar{k}_t^2\bar{k}_i^2 + m_0\omega^2L^6\right)}{\bar{k}_i\bar{k}_t^2\left(B_8\bar{k}_i^4 + 2c_2AL^2\bar{k}_i^2 + 2c_3AL^2\bar{k}_i^2 + B_7L^2\bar{k}_i^2 - 2\mu AL^4\right)}\mathcal{B}_i; \quad (i = 1, 2, 3, ...6)
\end{aligned} \tag{21}$$

With Eqs.(20) and (21), 24 equations concerning the amplitudes of each progressive and retrograde wave can be established. Then the amplitudes of transverse displacement $\overline{w}$ and rotation angle $\psi$ at the observation point on each frequency can be obtained.

## 5. Sound Radiation from the SSG theory based Timoshenko beam

Sound radiation from vibrating structures is of great impact on the surrounding environment. Sound radiation is generated by interactions between the structure and the ambient fluid, so it depends both on the structure dimensions, boundary conditions, material properties, external excitation, and ambient fluid properties. The SSG theory-based model enriches structural dynamic behavior with micro-structure characters, which will surely affect the resulting sound radiation. This section intends to analyze the sound radiation from the vibrating surface of the Timoshenko beam excited by a simple harmonic transverse force. Sound radiation from an infinite complex beam is analyzed concerning radiation impedance and radiated pressure field. Then sound radiation from a finite-sized complex beam with proper boundary conditions is calculated based on Kirchhoff-Helmholtz integral equation. The impact of the local behavior of heterogeneity on the radiation features of complex structures will be discussed by comparing the results from the SSG theory model and classical theory model.

*5.1. Sound radiation from infinite beam*

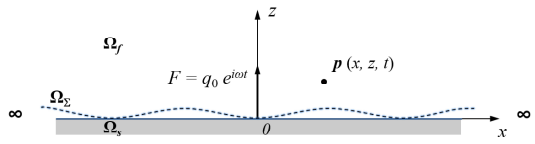


Figure 3: sound radiation from an infinite Timoshenko beam

As shown in Figure 3, the vibrating beam subject to a transverse harmonic force $F = \mathrm{Re}\left\{q_0 e^{i\omega t}\right\}$ at $x = 0$ is assumed to be infinitely extended along $x$ direction, and the waves generated by the vibrating surface $\Omega_\Sigma$ in the fluid domain $\Omega_f$ propagate away from the source at speed $c_0$. Acoustic wave motion equation governing the propagation of acoustic disturbances through a homogeneous, inviscid, isotropic, compressible fluid can be written in terms of the variation of pressure about the equilibrium pressure as

$$\frac{\partial^2 p}{\partial x^2} + \frac{\partial^2 p}{\partial y^2} + \frac{\partial^2 p}{\partial z^2} - \frac{1}{{c_0}^2}\frac{\partial^2 p}{\partial t^2} = 0. \tag{22}$$

where $p$ is the radiated acoustic pressure in the field, and $c_0$ represents the frequency-independent speed of sound govern by the fluid medium. In studying the sound radiation from beam structure to fluid, the vibration is uniform along the $y$ direction, so is the acoustic pressure field. Then the simplified two-dimensional wave propagation form is expressed in association with simple harmonic time dependence as,

$$\frac{\partial^2 p}{\partial x^2} + \frac{\partial^2 p}{\partial z^2} = -\left(\frac{\omega}{c_0}\right)^2 p = -k_0^2 p, \tag{23}$$

where $k_0 = \frac{\omega}{c_0}$. Since the vibration field is symmetrical about the force excitation point $x = 0$, the main attention is paid to the wave propagation field $x \geq 0$. According to the enriched Timoshenko beam model, the transverse velocity at the vibrating surface $x$ in region $[0, +\infty)$ can be expressed in wave superposition form as,

$$v_n(x,t) = i\omega \cdot w(x,t) = i\omega \cdot \left(\sum_{i=1}^{6} \mathcal{A}_i e^{-ik_i x}\right) \cdot e^{i\omega t}. \tag{24}$$

This complex solution represents all the physically possible forms for transverse vibration velocity of the surface, and each amplitude $\mathcal{A}_i$ can be expressed out in forms of the excitation force $q_0$ by FRF analysis. Generated by harmonic acceleration disturbance at the structure-fluid interface, the radiated acoustic pressure may also be expressed by the superposition of six acoustic pressure fields to physically represent the sound radiation from six wave modes generated at the source. Therefore the complex exponential form of the acoustic pressure $p(x,z,t)$ representing the propagation of sound pressure in the two-dimensional space $x \geq 0, z \geq 0$ is given as,

$$p(x,z,t) = \left(\sum_{i=1}^{6} \mathcal{R}_j \cdot e^{-i\left(k_{x_i} x + k_{z_i} z\right)}\right) \cdot e^{i\omega t}, \tag{25}$$

in which $k_{x_i}$ and $k_{z_i}$ represent the component of wavevector $\mathbf{k}_i$ in $x$ and $z$ direction generated by elastic wave $k_i$ in the solid. Substitute the solution of acoustic pressure $p(x,z,t)$ into (22), the relations of wavevector components constituting the radiated acoustic pressure field are expressed as

$$k_{x_i}^2 + k_{z_i}^2 = {k_0}^2; \quad (i = 1, 2, 3, ...6). \tag{26}$$

In deriving the wave equation, the linearised form of Euler momentum equations are used as

$$\nabla p + \rho_0 \frac{\partial \dot{\mathbf{u}}}{\partial t} = 0. \tag{27}$$

in which $\nabla p$, $\dot{\mathbf{u}}$ respectively denote the pressure gradient and particle velocity vector, and $\rho_0$ is the density of fluid. In $z$ direction, the vibration velocity $u_z$ of a point on the interface in fluid domain equals the transverse vibration velocity $v_n(x,t)$ at that point on the beam surface. Then with Euler momentum equation, the pressure gradient in $z$ direction in fluid domain can be connected with the particle acceleration of the structure normal to the interface between the two media as

$$\left.\frac{\partial p}{\partial z}\right|_{z=0} = -\rho_0 \cdot \left.\frac{\partial v_n}{\partial t}\right|_{z=0}. \tag{28}$$

Substitution of the solution form of acoustic pressure Eq. (25) and transverse displacement of the beam Eq. (24) into Eq. (28) yields the following relation,

$$\sum_{i=1}^{6} -ik_{z_i}\mathcal{R}_i \cdot e^{-ik_{x_i}x} = \rho_0 \cdot \omega^2 \cdot \left(\sum_{i=1}^{6} \mathcal{A}_i e^{-ik_i x}\right) \tag{29}$$

To have acoustic pressure solution for Eq. (29) on arbitrary frequency for arbitrary position, $k_{x_i}$ should take the same value with $k_i$ as

$$k_{x_i} = k_i, \quad (i = 1, 2, 3, ...6). \tag{30}$$

Combined with the above relation in Eq. (26), $k_{z_i}$ should take the values as,

$$k_{z_i} = \sqrt{{k_0}^2 - {k_i}^2}, \quad (i = 1, 2, 3, ...6). \tag{31}$$

To satisfy the Euler momentum in Eq. (29), the corresponding coefficients in front of component of each wave mode on both sides of the equation should be identical to each other. Hence the coefficients $\mathcal{R}_i$ in acoustic pressure solution are obtained as,

$$\mathcal{R}_i = \frac{i\rho_0\omega^2\mathcal{A}_i}{k_{z_i}} = \frac{i\rho_0\omega^2\mathcal{A}_i}{\sqrt{{k_0}^2 - {k_i}^2}}, \quad (i = 1, 2, 3, ...6). \tag{32}$$

Substitution of the obtained wavevectors and amplitudes into Eq. (25) yields the acoustic pressure in the radiation field $x \geq 0, z \geq 0$ from the enriched Timoshenko beam model as (omitting the time component $e^{i\omega t}$)

$$p(x,z,\omega) = \sum_{i=1}^{6} \left(\frac{i\rho_0\omega^2\mathcal{A}_i}{\sqrt{{k_0}^2 - {k_i}^2}} \cdot e^{-i\left(k_i x + k_{z_i} z\right)}\right) \tag{33}$$

A similar process can also be applied in calculating the solution of acoustic pressure in the region $x \leq 0, z \geq 0$.

The amplitude of the pressure field is determined by the application of the condition of compatibility of normal velocities or displacements at the structure fluid interface. The specific acoustic impedance of the fluid at the interface $Z(x,\omega)$ describing the relationship between the oscillator velocity perpendicular to the vibrating surface and the resulting acoustic pressure at that point generated by that surface as shown in Eq. (34)

$$Z(x,\omega) = \frac{p(x,0,\omega)}{v_n(x,\omega)} = \frac{\sum_{i=1}^{6}\left(\frac{i\rho_0\omega^2\mathcal{A}_i}{\sqrt{{k_0}^2-{k_i}^2}}\cdot e^{-ik_i x}\right)}{i\omega\cdot\left(\sum_{i=1}^{6}\mathcal{A}_i e^{-ik_i x}\right)} \tag{34}$$

The active energy that can be radiated into the ambient fluid from surface $S$ and the reactive energy stored in the near field of the source can be respectively expressed as

$$\begin{aligned} P_\Sigma &= \frac{1}{2}\int_S \mathrm{Re}\left\{p(x,0,\omega)\cdot\tilde{v}_n^*(x,\omega)\right\}dS = \frac{1}{2}\int_S \mathrm{Re}\left\{Z(x,\omega)\right\}\cdot\left|v_n(x,\omega)\right|^2 dS \\ Q_\Sigma &= \frac{1}{2}\int_S \mathrm{Im}\left\{p(x,0,\omega)\cdot\tilde{v}_n^*(x,\omega)\right\}dS = \frac{1}{2}\int_S \mathrm{Im}\left\{Z(x,\omega)\right\}\cdot\left|v_n(x,\omega)\right|^2 dS \end{aligned} \tag{35}$$

We can see real part of the impedance represents the energy that can be radiated into the ambient medium from surface $S$, while the imaginary part of the impedance represents the energy stored in the near field of the source, the square normal velocity of the vibrating surface can be regarded as an input to the energy radiation.

### *5.2. Sound radiation from simply supported beam in a rigid baffle*

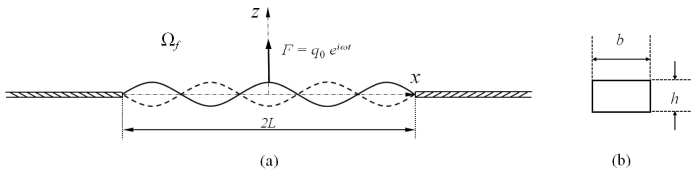


Figure 4: sound radiation from simply supported beam in a rigid baffle

As shown in Figure 4, one beam of length $2L$ embedded in an infinite rigid baffle in $x$ direction is considered. The beam is simply supported at both ends and excited by one harmonic force in the middle.

The vibration displacement can be described by a superposition of all the vibrating modes as

$$w(x,t) = \tilde{w}(x) \cdot e^{i\omega t} = \left( \sum_{i=1}^{6} \mathcal{A}_i e^{-ik_i x} + \sum_{i=1}^{6} \mathcal{B}_i e^{ik_i x} \right) \cdot e^{i\omega t}. \tag{36}$$

in which $\tilde{w}(x)$ represents the product summation of complex mode amplitude and modes, and amplitudes of each mode can be calculated out with FRF analysis. Then the surface vibration velocity distribution $v_n(x,\omega)$ is given as

$$v_n(x,\omega) = i\omega \cdot \tilde{w}(x) \cdot e^{i\omega t} = \tilde{v}_n \cdot e^{i\omega t}. \tag{37}$$

The total sound radiation due to the surface vibration can be physically regarded as the superposition of all the sound radiation fields generated by the progressive and retrograde modes, and each mode can be regarded as the superposition of several independent baffled piston cases. Therefore, the radiation from each mode could be estimated individually and then summed to give the total radiation pressure field. To estimate the pressure field of each mode, the direct boundary integral formulation based on the Kirchhoff–Helmholtz integral theorem is employed here. The pressure at a field point $\mathbf{r}$ in the interior or the exterior volume can be expressed in terms of the pressure $p(\mathbf{r})$ and the normal velocity $\tilde{v}_n$ at a boundary point $\mathbf{r}_a$ on the related closed boundary surface $S_a$ as

$$c(\mathbf{r})p(\mathbf{r}) = \iint_{S_a} \left( p(\mathbf{r}) \frac{\partial G(\mathbf{r},\mathbf{r}_a)}{\partial n} - G(\mathbf{r},\mathbf{r_a}) \frac{\partial p(\mathbf{r_a})}{\partial n} \right) dS_a; \tag{38}$$

where $c(\mathbf{r})$ is a coefficient dependent on the location of the field point. For the studied exterior problem, $c(\mathbf{r}) = -1$ is set. $n$ is the normal direction at the boundary surface directed to the fluid domain; $G$ is a Green's function satisfying the Helmholtz equation. In the following analysis, Green's function is applied to one unbounded fluid. Without scattering boundaries, the Green's function must satisfy the Sommerfeld radiation condition that only waves traveling outward from the point source are allowed and that the pressure tends to zero at an infinite distance from the source, one solution is

$$G(\mathbf{r},\mathbf{r}_a,\omega) = \frac{e^{-ik|\mathbf{r}-\mathbf{r}_a|}}{4\pi|\mathbf{r}-\mathbf{r}_a|} \tag{39}$$

Combined with Eq. (38), the acoustic pressure in any point $\mathbf{r}$ in the studied fluid domain $\Omega_f$ is determined by the combination of the pressure distribution $p(\mathbf{r}_a)$ and normal velocity distribution related with $\frac{\partial G}{\partial n}$ on the vibrating boundary surface $S_a$.

For the studied beam structure, assuming the pressure on each vibrating surface of are $S_a^+$ and $S_a^-$ is $p(\mathbf{r})$, Green's function on $S_a^+$ and $S_a^-$ is $G_{S_a}$, $\frac{\partial G}{\partial n}$ on $S_a^+$ and $S_a^-$ will have the same magnitude but different sign. Then the contribution of the first term, pressure distribution, will be necessarily canceled out. The only remaining term is the second term, the normal velocity distribution. The Green's function propagate the normal velocity which is related with $\frac{\partial p}{\partial n}$, from the surface. Then the pressure at any point in the

Table 1: High-order material constants for aluminum (Shodja et al.,2012).

| | | | | | | |
|---|---|---|---|---|---|---|
| $a_1$(eV/Å) | $a_2$(eV/Å) | $a_3$(eV/Å) | $a_4$(eV/Å) | $a_5$(eV/Å) | | |
| 0.1407 | 0.0027 | −0.0083 | 0.0966 | 0.2584 | | |
| $b_1$(eV/Å) | $b_2$(eV/Å) | $b_3$(eV/Å) | $b_4$(eV/Å) | $b_5$(eV/Å) | $b_6$(eV/Å) | $b_7$(eV/Å) |
| 0.7927 | 0.0644 | −0.1943 | −0.0009 | −0.0009 | 16.1566 | 48.5291 |
| $c_1$(eV/Å) | $c_2$(eV/Å) | $c_3$(eV/Å) | | | | |
| 0.5041 | 0.3569 | 0.1782 | | | | |

radiated field can be expressed purely in terms of the distribution of normal surface acceleration as

$$p(\mathbf{r}) = \iint_{S_a^+ + S_a^-} \left( G(\mathbf{r}, \mathbf{r_a}) \frac{\partial p(\mathbf{r_a})}{\partial n} \right) dS_a = \iint_{S_a^+} \left( -2i\rho_0 \omega G(\mathbf{r}, \mathbf{r_a}) \tilde{v}_n(\mathbf{r_a}) \right) dS_a; \tag{40}$$

For the studied SSG theory-based Timoshenko beam model, the pressure at point $(x', z')$ in the radiated fluid domain can be obtained by substituting the normal velocity distribution (37) and form of Green's function into the Kirchhoff Helmholtz integral Eq. (40) as (omitting the time component $e^{i\omega t}$)

$$p(x', z', \omega) = \frac{-i\rho_0 \omega}{2\pi} \int_{-L}^{L} \frac{e^{-ikR}}{R} \tilde{v}_n(x)\, dx; \tag{41}$$

in which $R = \sqrt{(x' - x)^2 + z'^2}$ represents the distance between the observation point $(x', z')$ and the source $(x, 0)$.

## 6. Numerical application and result discussion

Numerical cases are implemented in this section to illustrate the complex wave propagation and radiation behaviors as well as the impact of local behavior of heterogeneity in the complex media. The geometric shape of the beam is shown as in Figure 1. The material is assumed to be aluminum with $\mu = 26\,\text{GPa}$. The higher-order material constant values are given in Table 1, which refers to the work by Shodja et al. (2012) [23] with the atomistic approach. The beam's cross-section has width $b = 3h$, length $L = 5h$, and height of the section $h = 10a_0$, with the lattice parameter $a_0 = 4.04$Å.

### *6.1. Dispersion curves*

Employing the structural and material parameters into the dispersion relation in Eq. (8), one arrives 12 solutions which indicate 6 positive-going wave and 6 negative-going waves corresponding to each frequency. The dispersion curves of positive-going wave modes are shown in Figure 5.

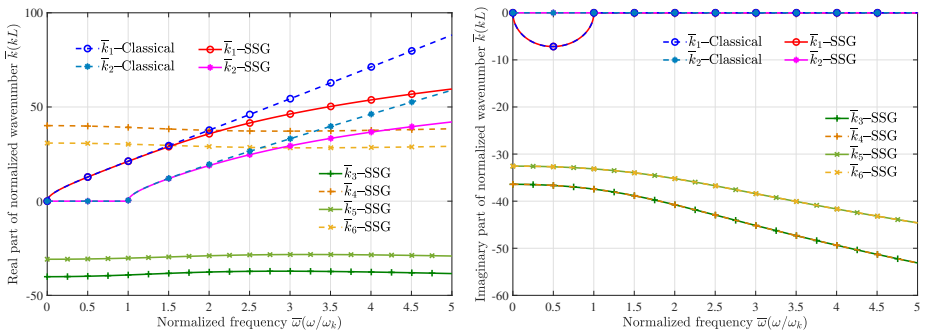


(a) Real part (b) Imaginary part

Figure 5: Dimensionless dispersion relation

Figure 5 displays the dispersion curves of the positive-going wave modes in the enriched model and classical model in frequency range $\overline{\omega} \in [0, 5]$. Fig. 5(a) and fig. 5(b) respectively show the real parts and imaginary parts. To be noted, the direction of propagation (positive-going or negative-going) is defined by the Imag $(k)$, which corresponds to the wave attenuation. The positive- or negative-going waves can have arbitrary Real $(k)$ sign. Thus wave $k_3$ and $k_5$, with negative imaginary part and negative real part are considered as positive-going waves.

Different from the dispersion relation in classical beam theory model, 6 wave modes $(k_1, k_2, k_3, k_4, k_6, k_6)$ are generated in the enriched Timoshenko beam model. $k_1$-SSG is non-classical bending wave and $k_2$-SSG is non-classical shear waves. $k_3$, $k_4$, $k_5$ and $k_6$ are the evanescent waves which exist exclusively in enriched model. Compared with $k_1$-Classical and $k_2$-Classical, $k_1$-SSG and $k_2$-SSG are less in value especially in higher frequency, therefore waves propagation in complex media exhibits longer spatial periodicity on the same frequency than classical media. For the other 4 evanescent waves, $k_3$ and $k_4$ are real part conjugate, so do $k_5$ and $k_6$. These four waves decay to zero in a very close range after being generated. They do not transport energy to a far-field but they do affect energy attenuation in the near field.

To confirm the size-effect feature in wave propagation, dispersion curves of non-classical bending wave $k_1$-SSG in the enriched model of different sizes are investigated. The results are illustrated in Figure 6.

As we can see in Figure 6, the resulting classical dispersion curve is size-independent, whereas the non-classical dispersion curves are observed to exhibit size-dependent features. The structure's height $h$ increases and deformation wavelength is proportional to $h$, therefore deformation wavelength becomes longer than the characteristic length of internal heterogeneity, and the influence of long-range interaction between internal micro-structures diminishes gradually. The enriched dispersion curve converges to the classical one in structure with fairly large dimensions. This is also the reason why the size effect can be observed in

nano-sized structures.

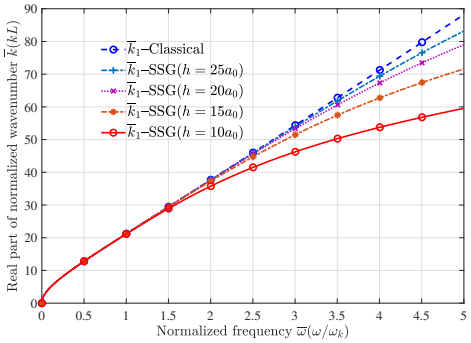


Figure 6: Bending wave dispersion curves changing with dimension

*6.2. modal density*

In the enriched model, only non-classical bending wave $k_1$-SSG and non-classical shear wave $k_2$-SSG can travel in long-distance and transfer energy to the far-field. Hence modal densities of these two waves are analyzed to study the statistical distribution of resonances of the enriched model in a higher frequency range.

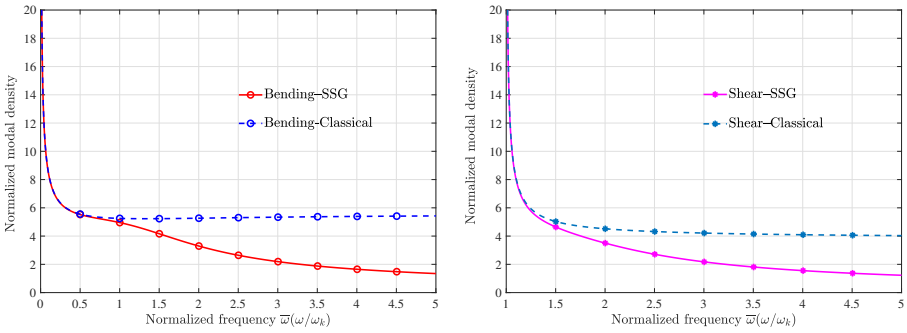


(a) Bending wave (b) Shear wave

Figure 7: Modal density of bending wave and shear wave

Fig. 7(a) and Fig. 7(b) respectively depict modal densities of bending wave and shear wave. To be noted here, the studied frequency range of shear wave is $\overline{\omega} \in [1, 5]$ as the shear wave propagate to far-field only above the cut-on frequency ($\overline{\omega}$¿1). In higher frequency, the obtained modal densities from SSG theory model declines distinctly compared with the classical ones, which indicates the expected number of

resonances is much less than the classical result on the same frequency. This difference comes from the less transferred energy in the system, which originates from the influence of long-range interaction between underlying micro-structures. In higher frequency, the deformation wavelength becomes more comparable to the internal characteristic length of the structure, therefore the influence of internal micro-structures becomes more distinct.

### *6.3. Energy velocity*

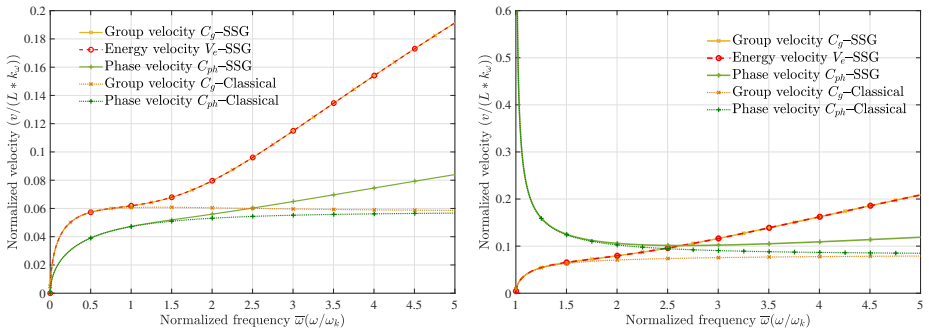


(a) Bending wave (b) Shear wave

Figure 8: Energy velocity of bending wave and shear wave

In section 3.3, energy flow expression for SSG theory-based beam model is established. The validation of energy flow expression is important for the following research as knowledge of energy transportation pathway are fundamental to build energy equilibrium. Figure 8 depicts the energy velocity $\mathrm{V}_e$, group velocity $C_g$ and phase velocity $C_{ph}$ of bending wave and shear wave resulting from SSG theory model and classical theory model. ***The formulation of potential energy*** (16) ***and energy flow*** (17) ***in the enriched model are proved to be correct with*** $C_g = \mathrm{V}_e$ ***for both bending wave and shear wave in the whole frequency range.*** In addition, the results of the classical model and enriched model match well in the low-frequency range ($\overline{\omega} < 1$ for bending wave and $\overline{\omega} < 1.5$ for shear wave). As frequency increases, $\mathrm{V}_e$-Classical for both bending wave and shear wave approach to one constant value, whereas $\mathrm{V}_e$-SSG of non-classical waves keep increasing. Therefore, energy velocities of non-classical waves $\mathrm{V}_e$-SSG are larger than the classical ones in higher frequency. Meanwhile, phase velocity $C_{ph}$-SSG is also increasing with frequency and larger than $C_{ph}$-Classical. The wider gap between $C_g$-SSG and $C_{ph}$-SSG in high frequency implies the more distinct dispersive character for both bending wave and shear wave propagating in the enriched model.

### 6.4. Frequency response analysis

The numerical investigation of frequency response is proceeded with the amplitude of excitation force $q_0 = 0.05\mu A$ at $x = L$.

#### 6.4.1. Wave approach result

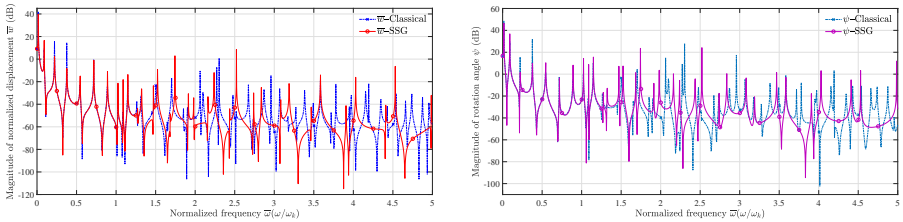


(a) Frequency response of $\overline{w}$ (b) Frequency response of $\psi$

Figure 9: Frequency response of $\overline{w}$ and $\psi$

Figure 9 displays the normalized deflection amplitude $\overline{w}$ and rotation amplitude $\psi$ at observation point $x = 0.7L$ in Timoshenko beam. As we can see, the enriched frequency responses match well with the classical results in the first about 10 resonances as the wavelength generated by the excitation is much larger than the internal characteristic length of the beam. In higher frequency, fewer resonance peaks can be observed in complex beam structures. In terms of energy, the input vibration energy can not only be transferred by the propagating waves but also be converted into the other evanescent waves which decay rapidly in the near field of the excitation. The active power is distinctively less, so wave propagation features, as well as the dynamic behavior of the complex structure, are affected. This can be the interpretation for the reduction of resonance peaks. As frequency increase, wavelength generated by the excitation decrease and becomes more comparable with the internal characteristic length of the media. Therefore micro-structure effects are more prominent, and the resulting frequency response shows more difference with the classical model.

#### 6.4.2. Frequency response analysis in COMSOL

As we can see in Figure 10, the frequency response resulting from COMSOL matches well with frequency response with wave approach. The previous formulations are proven to be rigorous and the result is validated. With the analytical governing equations deduced based on generalized elasticity theory and proper input in weak form, COMSOL can be employed to calculate the structural response of complex media with less computational effort and a wider frequency range.

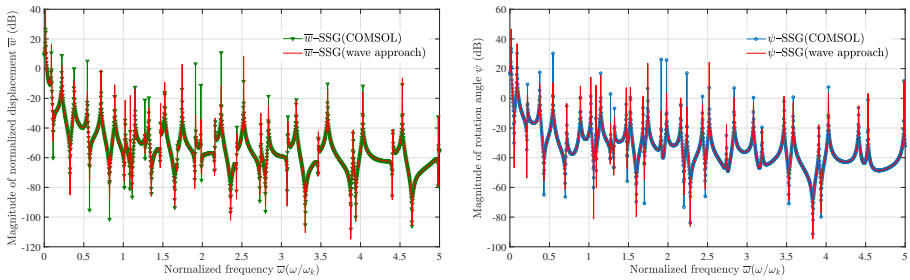


(a) Frequency response of $\overline{w}$ (b) Frequency response of $\psi$

Figure 10: Frequency response of $\overline{w}$ and $\psi$ in COMSOL

### *6.5. Sound radiation analysis*

#### *6.5.1. Sound radiation from an infinite enriched model*

The numerical case is proceeded to study sound radiation features from an infinite complex beam structure based on the previous enriched model. Media in the fluid domain is set to be air with density $\rho_0 = 1.2\text{kg/m}^3$ and sound velocity $c_0 = 343\text{m/s}$. Amplitude of the harmonic transverse force $q_0 = 0.1\mu A$ at $x = 0$ in Figure 3. The transverse displacement, as well as the square normal velocity of the vibrating surface, can be obtained by FRF analysis.

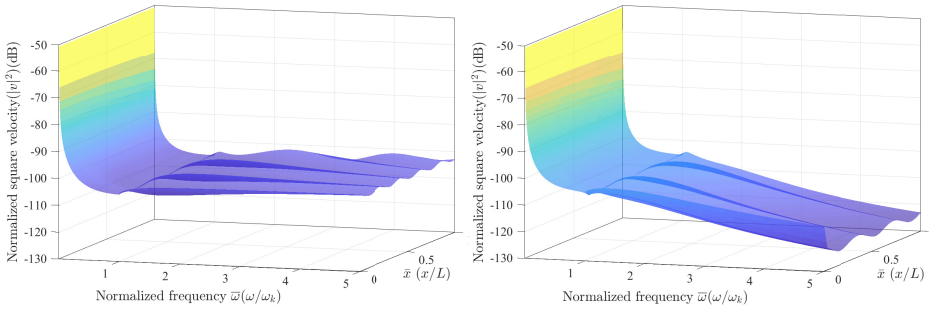


(a) Square velocity (CT) (b) Square velocity (SSG)

Figure 11: Transverse square velocity of the vibrating beam

Figure 11 illustrates the square normal velocity of the vibration surface in space interval $[0, 1]$ in frequency range $\overline{\omega} \in [0, 5]$. We can see $|v_n|^2$ of the classical model varies spatially simply in sine form In higher frequency range $1 < \overline{\omega} < 5$ as shown in Figure 11(a). In contrast, $|v_n|^2$-SSG is generated to be less than the classical one at $\overline{x} = 0$ in Figure 11(b), drops distinctly in the near field of excitation point and then varies sinusoidally

in the far-field. The higher the frequency, the more distinct the decrease in the near field. Therefore, $|v_n|^2$ of the SSG theory is lower than the classical result. The lower square velocity at $\overline{x} = 0$ is caused by energy converting to evanescent wave modes in the enriched model, and the decrease of $|v_n|^2$ in the near field is caused by the rapid decay of evanescent waves in close distance.

The input normal velocity together with radiation impedance determine the radiated energy, thus the decrease of normal velocity in the near field will significantly affect the acoustic radiation to the fluid domain. To display the enriched pressure field and radiation impedance systematically, radiation impedance ($\overline{Z}$) on structure fluid interface $\Omega_\Sigma$ in the region $0 < \overline{x} < 1$ is illustrated in Figure 12.

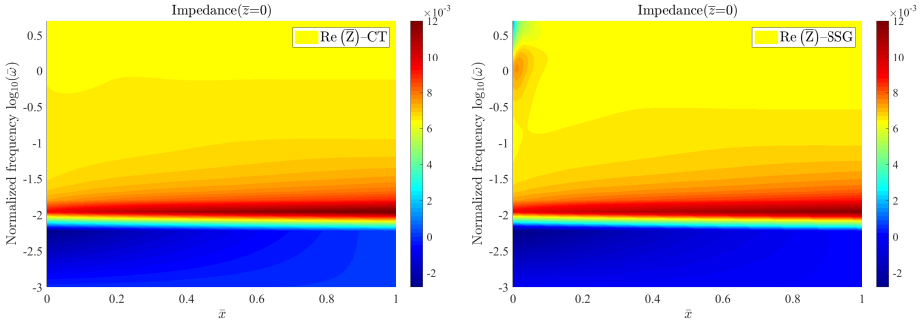


(a) Acoustic impedance (CT) (b) Acoustic impedance (SSG)

Figure 12: Acoustic radiation impedance

Figure 12 illustrates the real part of radiation impedance, which represents the energy that can be radiated into the fluid domain. As we can see, the first peak of radiation impedance arises at the frequency when $k_{z_1}$ (generated by bending wave) changes from pure imaginary value to pure real value on the critical frequency $\omega_r$, then radiation of bending wave becoming effective. This peak arises for both classical beam model and enriched beam model on the entire spatial position $\overline{x} \in [0, 1]$. The different behavior of the enriched beam is that another relatively small peak arises in the near field of excitation on a high frequency. This small peak is caused by variation of $k_{z_i}$ $(i = 3, 4, 5, 6)$ from attenuating in the near field to propagating to far-field. This $k_{z_i}$ $(i = 3, 4, 5, 6)$ corresponds to the evanescent waves in the enriched model, so the small impedance peak appears exclusively in the near field of the force excitation. If the observation point is moving to the far-field (i.e. $\overline{x} > 0.2$), the second peak becomes gentle and eventually disappears.

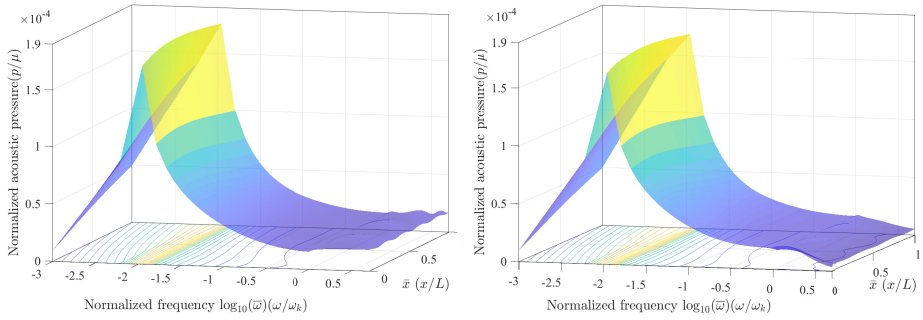


(a) Acoustic pressure (CT) (b) Acoustic pressure (SSG)

Figure 13: Acoustic pressure amplitude

Radiation pressure modulus $|\overline{p}|$ on the structure fluid interface $\Omega_\Sigma$ in region $0 < \overline{x} < 1$ is shown in Figure 13. The peak appearing in a low-frequency domain for both the classical and the enriched model is governed by the critical frequency $\omega_r$ on which $k_{z_1}$ transfers from pure imaginary to pure real value. In higher frequency range when $log10(\overline{\omega}) > 0$, namely $\overline{\omega} > 1$, $|\overline{p}|$ – SSG is obviously decreasing as frequency increases, this decrease is resulting not only from the less input normal velocity but also the second peak of enriched radiation impedance.

To illustrate the radiation pressure field of the SSG theory-based Timoshenko beam varying in $x - z$ plan and study the impact of the extra evanescent waves in complex media, the radiation pressure field of classical theory model and SSG theory model in the region $\overline{x} \in [0 - 1], \overline{z} \in [0, 10]$ at different frequencies ($\omega$=0.5, 1.5 and 2.5) are plotted in Figure 14.

Comparison of pressure field on each frequency yields the impact of the enrichment by the micro-structure character on structural radiation behavior. Firstly, the enriched radiation pressure field on frequency $\overline{\omega} = 0.5$ matches well with the classical result, it is reasonable because the influence of microstructure is less important in the low-frequency range. On frequency $\overline{\omega} = 1.5$, the pressure amplitude of the enriched model is lower than the classical one. This difference becomes more remarkable when frequency increases to $\overline{\omega} = 2.5$. In higher frequency, the wavelength is more comparable with the characteristic size of underlying micro-structures, therefore the resulting influence becomes more prominent. Moreover, the highest pressure in SSG theory radiation field on frequency $\overline{\omega} = 2.5$ is near the energy input point at $\bar{x} = 0$, but after being generated, the radiated pressure decreases rapidly in the near field.

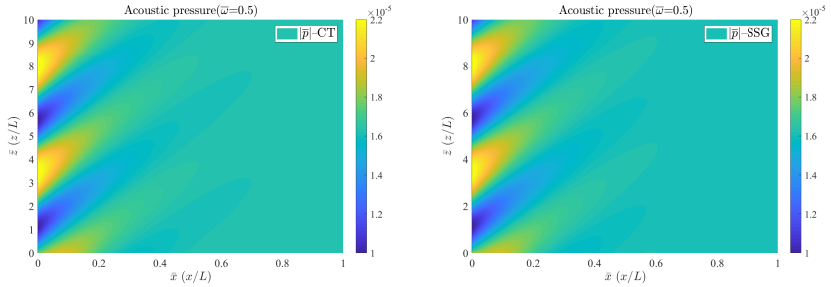


(a) Classical pressure field $\overline{\omega} = 0.5$




(b) Enriched pressure field $\overline{\omega} = 0.5$

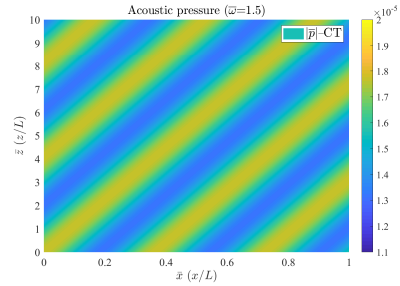


(c) Classical pressure field $\overline{\omega} = 1.5$

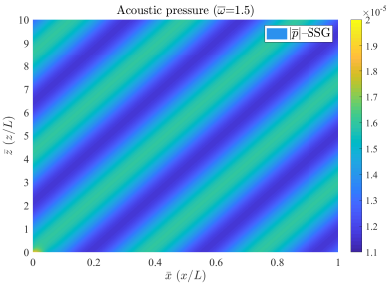


(d) Enriched pressure field $\overline{\omega} = 1.5$

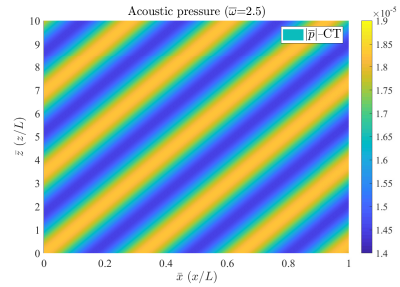


(e) Classical pressure field $\overline{\omega} = 2.5$

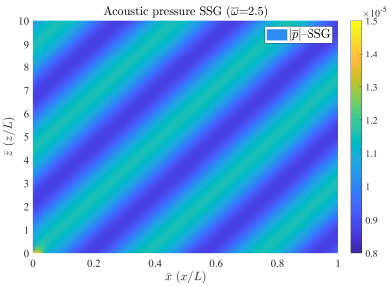


(f) Enriched pressure field $\overline{\omega} = 2.5$

Figure 14: Radiation pressure in $x - z$ plane

To study the drop of pressure in the near field of force excitation, SSG theory-based pressure fields in region $x \in [0 - 0.1], z \in [0 - 1]$ are illustrated respectively on frequency $\overline{\omega} = 1.5$ and 2.5 in Figure 15.

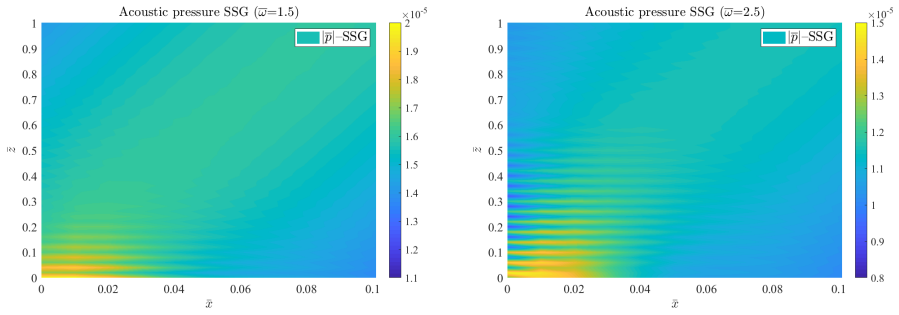


(a) $\overline{\omega} = 1.5$ (b) $\overline{\omega} = 2.5$

Figure 15: Near field of enriched radiation pressure field

As we can see, the radiated pressure decreases rapidly with some slight fluctuation in the near field. This phenomenon is the decay of short waves generated by the evanescent waves in a complex structure, which originate with the long-range interactions between underlying micro-structures. After being generated by the vibrating surface, sound pressure firstly decays rapidly to some extent in the near field then propagates away to infinity. Therefore we can say that the enrichment of micro-structure interaction character by SSG theory can successfully capture the distinct radiation behavior of the complex media.

### *6.6. Sound radiation from simple supported Timoshenko beam based on SSG theory*

In the numerical study of sound radiation from finite beam structure, the fluid is also set to be air, and half of the beam length $L = 10h$. Amplitude of the harmonic axial force $q_0 = 0.01\mu A$ at $x = 0$ in Figure 4. Substitute the parameters into the formulation, the transverse displacement, as well as normal velocity of the vibrating surface, can be obtained by FRF analysis, then the radiated pressure field can be calculated out with the integral equation Eq. (41).

Figure 16 shows the radiated pressure field on frequency $\overline{\omega} = 0.1$ and the corresponding structure vibration shape of the classical beam and enriched beam. The frequency is in the low-frequency range, and the deformation wavelength is quite longer than the characteristic length of internal micro-structures, therefore the influence of microstructure is negligible, and results of classical model and SSG theory model math well in terms of both structural vibration shape and radiation pressure.

Figure 17 illustrates the radiated pressure field on frequency $\overline{\omega} = 1.5$ and the corresponding structure vibration shape for both classical beam and enriched beam. The frequency is higher and the deformation wavelength generated by excitation is comparable to the inner microstructure, thus amplitudes of radiation pressure as well as structural vibration decrease distinctly.

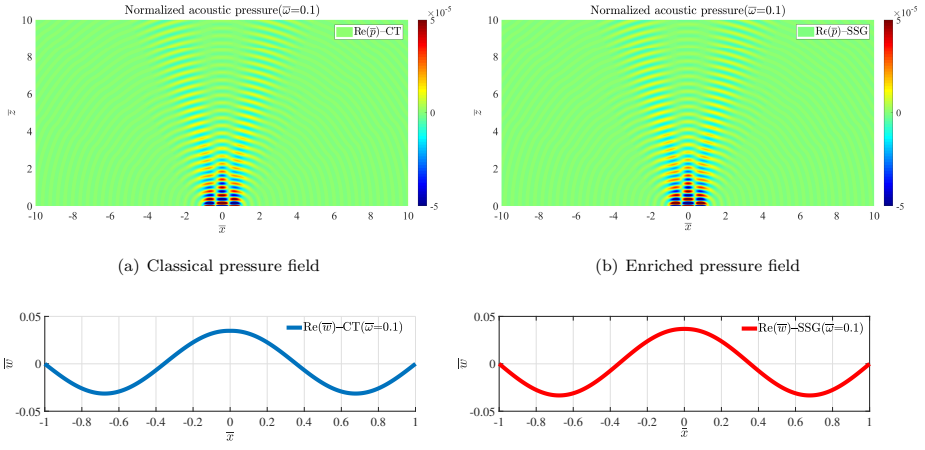


(a) Classical pressure field (b) Enriched pressure field

(c) Classical vibration structure shape (d) Enriched vibration structure shape

Figure 16: Acoustic pressure field and corresponding transverse displacement of classical model and enriched model($\overline{\omega} = 0.1$)

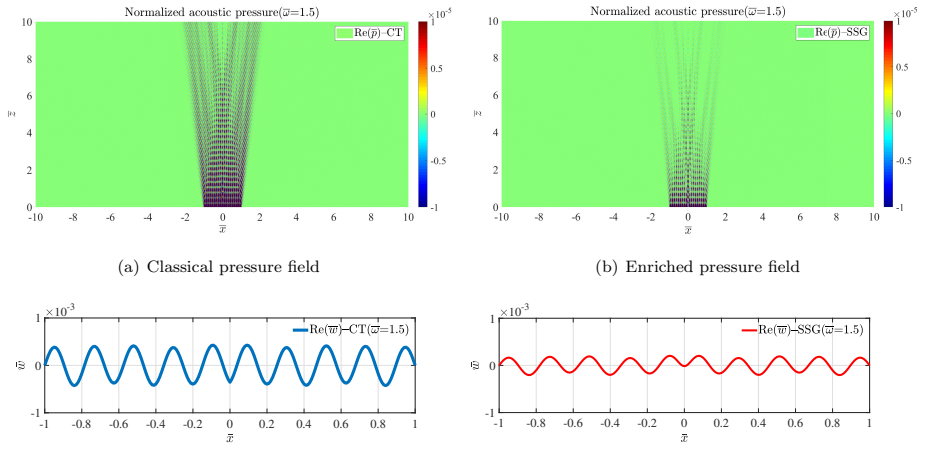


(a) Classical pressure field (b) Enriched pressure field

(c) Classical vibration structure shape (d) Enriched vibration structure shape

Figure 17: Acoustic pressure field and corresponding transverse displacement of classical model and enriched model ($\overline{\omega} = 1.5$)

## 7. Conclusions

Wave propagation in the SSG theory-based model with considering local behaviors of internal heterogeneity is different from the classical one. An extended Timoshenko beam theory was employed and studied

further under dynamic conditions. Precisely important vibroacoustic indicators were considered for the study. The enriched model based on Mindlin's SSG theory allows the underlying microstructure interaction to be captured by including the higher-order strains into strain energy density, meanwhile the local behavior of heterogeneity to be described in the frame of continuum mechanics. From the numerical calculations, one can see that the proposed SSG theory-based beam model is effective in predicting the non-classical dispersive behaviors in complex media. Apart from the dispersion characteristics, this research also highlighted a number of interesting features including the modal density, the formulation of energy flow, the frequency response function, and sound radiation from the beam structure. Some conclusions can be drawn from the numerical calculation and discussions as follows:

(1) Six wave modes can be generated in the enriched Timoshenko beam model based on SSG theory, of which the non-classical bending wave $k_1$ and non-classical shear wave $k_2$ propagate in a dispersive manner, and the dispersive behavior become more prominent in higher frequency. The other 4 waves are all evanescent waves (near field). Modal densities of the non-classical bending wave and non-classical shear wave are lower than the classical ones due to the influence of the micro-structure effect. As dimension goes up, the micro-structural effect is weakened due to the increase of structural characteristic length. Consequently, the non-classical results converges to the classical ones.

(2) The proposed formulation of the energy flow is validated, as the energy velocity $V_e$ and group velocity $C_g$ of conservative waves are proved to be identical in the whole frequency range. Energy flow in the enriched Timoshenko beam model based on SSG theory is a combination of work by the classical force, the classical moment along with the higher-order forces and higher-order moments, which are all resultants of classical and higher-order stresses generated on the surface of the observed section.

(3) From the FRF analysis, the first few resonances match well with the classical result. In a higher frequency range, when the deformation wavelength is comparable with the inner micro-structure length, fewer resonance peaks can be observed. Due to the complex interaction between internal micro-structures, the input vibration energy can not only be transferred to the far-field by the propagating waves but also be converted into the evanescent waves which will decay rapidly in the near field. The transfer power is distinctively less, thus the resonant frequency of the complex structure is affected.

(4) Concerning the noise radiation, the square velocity of the vibrating surface is lower than the classical one, which is attributed to lower force driving mobility and evanescent waves decaying in the near field of excitation point. The second peak of radiation impedance can be observed exclusively in the near field of excitation in enriched model, which originates with wavevector generated by the evanescent waves. Another interesting phenomenon is that radiated pressure field decreases with fluctuation in the near field of force excitation. This phenomenon is caused by the decay of short waves (generated by evanescent waves) in the fluid domain. Therefore we can conclude that the radiation level from the enriched model is lower caused by firstly less vibrating energy input, then sound wave decay in the near field. The underlying physics lies in

the distinct local behavior of heterogeneity in complex media governed by both near range and long-range micro-structure interactions.

(5) Radiation pressure from the finite enriched model is determined by the normal velocity of all the points on the vibrating surface. The resulting radiation pressure of the enriched model matches with the classical one in low frequency but is much lower than the classical one in higher frequency. The sound pressure reduction is caused by not only the reduced normal velocity of the vibrating surface but also the energy decay through the evanescent waves in the enriched model.

Finally, with regards to the question: *The main question being, how local behavior affects the vibroacoustic indicators and for what expected benefit?*, our conclusions clearly show that there is an important impact of the local behavior with regards to vibroacoustic indicators. This trend can provide a means to improve the design of lightweight structures while considering specific materials.

**Acknowledgement**

This work was supported by the LabEx CeLyA (Centre Lyonnais d'Acoustique, ANR-10-LABX-0060) of Université de Lyon. Guang ZHU thanks a scholarship provided by the China Scholarship Council.

## Appendix A: Frequency response analysis with FEM in COMSOL

$$
\begin{aligned}
&\frac{\partial}{\partial\bar{x}}\overline{V}_0+\bar{q}=m_0\frac{\partial^2\bar{w}}{\partial\tau^2}\\
&\overline{V}_0=-\psi-\left(\frac{(c_3+2c_2)\,A}{2\mu AL^2}\right)\left(\frac{\partial\psi_1}{\partial\bar{x}}\right)+\left(\frac{\partial\bar{w}}{\partial\bar{x}}\right)+\frac{c_3A}{2\mu AL^2}\left(\frac{\partial w_2}{\partial\bar{x}}\right)-\left(\frac{\partial\overline{V}_1}{\partial\bar{x}}\right)\\
&\overline{V}_1=\left(\frac{B_7}{2\mu AL^2}\right)\left(\frac{\partial\psi}{\partial\bar{x}}\right)+\frac{B_5}{\mu AL^2}\left(\frac{\partial w_1}{\partial\bar{x}}\right)-\left(\frac{\partial\overline{V}_2}{\partial\bar{x}}\right)\\
&\overline{V}_2=-\frac{c_3A}{2\mu AL^2}\psi+\frac{B_8}{2\mu AL^4}\left(\frac{\partial\psi_1}{\partial\bar{x}}\right)+\left(\frac{c_3A}{2\mu AL^2}\right)\left(\frac{\partial\bar{w}}{\partial\bar{x}}\right)+\frac{B_6}{\mu AL^4}\left(\frac{\partial w_2}{\partial\bar{x}}\right)\\
&w_1=\frac{\partial\bar{w}}{\partial\bar{x}},\qquad\overline{w}_2=\frac{\partial^2\bar{w}}{\partial\bar{x}^2}.\\
&-\psi+\frac{\partial}{\partial\bar{x}}\left(\overline{M}_0-\frac{(2c_2+c_3)\,A}{2\mu AL^2}\left(\frac{\partial\psi}{\partial\bar{x}}\right)+\bar{w}+\frac{c_3A}{2\mu AL^2}\left(\frac{\partial w_1}{\partial\bar{x}}\right)\right)=m_2\left(\frac{\partial^2\psi}{\partial\tau^2}\right);\\
&\overline{M}_0=\frac{B_1}{\mu AL^2}\left(\frac{\partial\psi}{\partial\bar{x}}\right)+\frac{B_4}{2\mu AL^4}\left(\frac{\partial\psi_2}{\partial\bar{x}}\right)+\frac{B_7}{2\mu AL^2}\left(\frac{\partial w_1}{\partial\bar{x}}\right)-\frac{\partial\overline{M}_1}{\partial\bar{x}},\\
&\overline{M}_1=\frac{(2c_2+c_3)\,A}{2\mu AL^2}\psi+\frac{B_2}{\mu AL^4}\left(\frac{\partial\psi_1}{\partial\bar{x}}\right)-\frac{(c_3+2c_2)\,A}{2\mu AL^2}\left(\frac{\partial\bar{w}}{\partial\bar{x}}\right)+\frac{B_8}{2\mu AL^4}\left(\frac{\partial w_2}{\partial\bar{x}}\right)-\frac{\partial\overline{M}_2}{\partial\bar{x}}\\
&\overline{M}_2=\frac{B_4}{2\mu AL^4}\left(\frac{\partial\psi}{\partial\bar{x}}\right)+\frac{B_3}{\mu AL^6}\left(\frac{\partial\psi_2}{\partial\bar{x}}\right);\\
&\psi_1=\frac{\partial\psi}{\partial\bar{x}},\qquad\psi_2=\frac{\partial^2\psi}{\partial\bar{x}^2}.
\end{aligned}
\tag{42}
$$

To verify the FRF results with the wave approach, the frequency response analysis of the enriched model is implemented in COMSOL. The governing equations of six order partial difference is transformed to eq. (42) and input in a weak form. The shape function used for discretization is six-tic Hermite polynomials to guarantee higher-order derivative continuity. Then the solution of each variable can be calculated including transverse displacement $\overline{w}$ and rotation angle $\psi$ at the observation point.

## References


[1] D. A. Bonnell, R. Shao, Local behavior of complex materials: scanning probes and nano structure, Current Opinion in Solid State and Materials Science 7 (2) (2003) 161 – 171. doi:https://doi.org/10.1016/S1359-0286(03)00047-0.

[2] M. Jirásek, Nonlocal theories in continuum mechanics, Acta Polytechnica 44 (5) (2004) 16 – 34. doi:https://doi.org/10.14311/610.

[3] M. Asghari, M. Kahrobaiyan, M. Ahmadian, A nonlinear timoshenko beam formulation based on the modified couple stress theory, International Journal of Engineering Science 48 (12) (2010) 1749–1761. doi:https://doi.org/10.1016/j.ijengsci.2010.09.025.
URL https://www.sciencedirect.com/science/article/pii/S0020722510002107

[4] R. Joseph, B. Wang, B. Samali, Size effects on double cantilever beam fracture mechanics specimen based on strain gradient theory, Engineering Fracture Mechanics 169 (2017) 309 – 320. doi:https://doi.org/10.1016/j.engfracmech.2016.10.013.

[5] R. D. Mindlin, Second gradient of strain and surface-tension in linear elasticity, International Journal of Solids and Structures 1 (4) (1965) 417 – 438. doi:https://doi.org/10.1016/0020-7683(65)90006-5.

[6] Y. Chen, J. D. Lee, Connecting molecular dynamics to micromorphic theory. (i). instantaneous and averaged mechanical variables, Physica A: Statistical Mechanics and its Applications 322 (2003) 359–376. doi:https://doi.org/10.1016/S0378-4371(02)01921-0.
URL https://www.sciencedirect.com/science/article/pii/S0378437102019210

[7] Q. Wang, K. Liew, Application of nonlocal continuum mechanics to static analysis of micro- and nano-structures, Physics Letters A 363 (3) (2007) 236–242. doi:https://doi.org/10.1016/j.physleta.2006.10.093.
URL https://www.sciencedirect.com/science/article/pii/S0375960106017154

[8] J. Yan, K. Liew, L. He, Free vibration analysis of single-walled carbon nanotubes using a higher-order gradient theory, Journal of Sound and Vibration 332 (15) (2013) 3740 – 3755. doi:https://doi.org/10.1016/j.jsv.2013.02.004.
URL http://www.sciencedirect.com/science/article/pii/S0022460X13000977

[9] H. T. Thai, D. H. Choi, Size-dependent functionally graded kirchhoff and mindlin plate models based on a modified couple stress theory, Composite Structures 95 (2013) 142 – 153. doi:https://doi.org/10.1016/j.compstruct.2012.08.023.
URL http://www.sciencedirect.com/science/article/pii/S0263822312003893

[10] R. Chebakov, J. Kaplunov, G. A. Rogerson, A non-local asymptotic theory for thin elastic plates, Proceedings of the Royal Society A: Mathematical, Physical and Engineering Sciences 473 (2203) (2017) 20170249. doi:10.1098/rspa.2017.0249.

[11] A. S. J. Suiker, R. de Borst, C. S. Chang, Micro-mechanical modelling of granular material. part 1: Derivation of a second-gradient micro-polar constitutive theory, Acta Mechanica 149 (1) (2001) 161–180. doi:10.1007/BF01261670.

[12] A. S. J. Suiker, R. de Borst, C. S. Chang, Micro-mechanical modelling of granular material. part 2: Plane wave propagation in infinite media, Acta Mechanica 149 (1) (2001) 181–200. doi:10.1007/BF01261671.
URL https://doi.org/10.1007/BF01261671

[13] S. Gopalakrishnan, Propagation of elastic waves in nanostructures, in: Nanosensors, Biosensors, and Info-Tech Sensors and Systems 2016, Vol. 9802, 2016, p. 98020N. doi:10.1117/12.2218203.

[14] L. Li, Y. jin Hu, L. Ling, Flexural wave propagation in small-scaled functionally graded beams via a nonlocal strain gradient theory, Composite Structures 133 (2015) 1079 – 1092. doi:https://doi.org/10.1016/j.compstruct.2015.08.014.
URL http://www.sciencedirect.com/science/article/pii/S0263822315006911

[15] A. V. Metrikine, H. Askes, One-dimensional dynamically consistent gradient elasticity models derived from a discrete microstructure: Part 1: Generic formulation, European Journal of Mechanics - A/Solids 21 (4) (2002) 555 – 572. doi:https://doi.org/10.1016/S0997-7538(02)01218-4.

[16] H. Askes, A. V. Metrikine, One-dimensional dynamically consistent gradient elasticity models derived from a discrete microstructure: Part 2: Static and dynamic response, European Journal of Mechanics - A/Solids 21 (4) (2002) 573 – 588. doi:https://doi.org/10.1016/S0997-7538(02)01217-2.
URL http://www.sciencedirect.com/science/article/pii/S0997753802012172

[17] I. Elishakoff, J. Kaplunov, E. Nolde, Celebrating the Centenary of Timoshenko's Study of Effects of Shear Deformation and Rotary Inertia, Applied Mechanics Reviews 67 (6). doi:10.1115/1.4031965.
URL https://doi.org/10.1115/1.4031965

[18] E. Nolde, A. V. Pichugin, J. Kaplunov, An asymptotic higher-order theory for rectangular beams, Proceedings of the Royal Society A: Mathematical, Physical and Engineering Sciences 474 (2214) (2018) 20180001. doi:10.1098/rspa.2018.0001.

[19] M. Asghari, S. Momeni, R. Vatankhah, The second strain gradient theory-based timoshenko beam model, Journal of Vibration and Control 23 (13) (2017) 2155–2166. doi:10.1177/1077546315611822.

[20] G. Zhu, C. Droz, A. Zine, M. Ichchou, Wave propagation analysis for a second strain gradient rod theory, Chinese Journal of Aeronauticsdoi:https://doi.org/10.1016/j.cja.2019.10.006.
URL http://www.sciencedirect.com/science/article/pii/S1000936119304091

[21] Y. Lase, M. Ichchou, L. Jezequel, Energy flow analysis of bars and beams: Theoretical formulations, Journal of Sound and Vibration 192 (1) (1996) 281 – 305. doi:https://doi.org/10.1006/jsvi.1996.0188.
URL http://www.sciencedirect.com/science/article/pii/S0022460X96901881

[22] M. N. Ichchou, A. L. Bot, L. Jezequel, Energy models of one-dimensional multipropagative systems, Journal of Sound and Vibration 201 (5) (1997) 535 – 554. doi:https://doi.org/10.1006/jsvi.1996.0780.

[23] M. Shodja, F. Ahmadpoor, A. Tehranchi, Calculation of the additional constants for fcc materials in second strain gradient elasticity: Behavior of a nano-size bernoulli-euler beam with surface effects, Journal of Applied Mechanics 79 (2) (2012) 1008–1016. doi:10.1115/1.4005535.

# Highlights

- Investigating the wave dispersion relation of SSG theory-based Timoshenko beam.
- Formulating and validating the expression energy flow in the enriched model.
- Studying the FRF and noise radiation based on the enriched model.
- Physical interpretation of the exhibited complex properties.
- Validation of FRF result with numerical method.

## AUTHORSHIP STATEMENT

Manuscript title: Sound radiation analysis with an enriched Timoshenko beam model based on second strain gradient theory

**Guang Zhu:** Methodology, Software, Investigation, Validation, Data Curation, Writing - Original Draft, Writing - Review & Editing, Visualization.

**Pascal Fossat**: Software, Investigation, Validation.

**Abdelmalek Zine**: Conceptualization, Methodology, Supervision.

***Mohamed Ichchou****:* Conceptualization, Methodology, Supervision, Project administration, Funding acquisition.

**Declaration of interests**

☒ The authors declare that they have no known competing financial interests or personal relationships that could have appeared to influence the work reported in this paper.

☐The authors declare the following financial interests/personal relationships which may be considered as potential competing interests: